

# Smoothed particle hydrodynamics: theory and application to non-spherical stars

R. A. Gingold and J. J. Monaghan<sup>★</sup> *Institute of Astronomy,  
Madingley Road, Cambridge, CB3 0HA*

Received 1977 May 5, in original form February 2

**Summary.** A new hydrodynamic code applicable to a space of an arbitrary number of dimensions is discussed and applied to a variety of polytropic stellar models. The principal feature of the method is the use of statistical techniques to recover analytical expressions for the physical variables from a known distribution of fluid elements. The equations of motion take the form of Newtonian equations for particles. Starting with a non-axisymmetric distribution of approximately 80 particles in three dimensions, the method is found to reproduce the structure of uniformly rotating and magnetic polytropes to within a few per cent. The method may be easily extended to deal with more complicated physical models.

## 1 Introduction

Many of the most interesting problems in astrophysics involve systems with large departures from spherical symmetry. This may occur either because the initial state lacks spherical symmetry, as in the case of a protostar forming from a dense interstellar cloud, or because non-spherical forces arising from rotation or magnetic fields, as in the case of the fission of a rotating star, play an important part in the dynamics. Frequently these sources of non-spherical symmetry will be found combined.

Because of the complexity of these systems numerical methods are required to follow their evolution. However, the standard finite difference representations of the continuum equations are of limited use, because of the very large number of grid points required to treat each coordinate on an equal footing. If, for example, 20 points along the radial direction give adequate accuracy for a spherical polytrope, we may require  $(20)^3$  such points to give the same accuracy for a highly distorted polytrope. This difficulty is mirrored in the evaluation of multiple integrals.

For the astrophysical problems a numerical method which allows reasonable accuracy for a small number of points is required. Ideally it should also be simple to program and robust. An early attempt to provide such an alternative to the standard finite difference method was made by Pasta & Ulam (1959). They replaced the continuous fluid by a fictitious set of

<sup>★</sup>Permanent address: Mathematics Department, Monash University, Clayton, Victoria 3168, Australia.

particles with inter-particle forces designed to mimic the true pressure and other body forces. The weakness in this method is that transport processes are difficult to include correctly.

A better method is to make use of the Lagrangian description of fluid flow which automatically focuses attention on fluid elements. In the discrete version, parcels of fluid move according to the Newtonian equations with forces due to the pressure gradient and other body forces: gravity, rotation and magnetic. The central feature of our analysis\* is the method we use to determine the forces from the current positions of the fluid elements.

For fluid elements of equal mass, the number per unit volume must be proportional to the density. In addition, unless special symmetry is introduced from the start, the positions of the elements will be random because of the complicated motion which is inevitable for large  $N$ -body systems. We therefore make the assumption that, at any time, the positions of the fluid elements are randomly distributed according to the density. To recover the density from the known distribution of elements is then equivalent to recovering a probability distribution from a sample. Statisticians have given two methods for doing this which are well suited to the fluid problem. The first is the smoothing kernel method (Bartlett 1963; Parzen 1962), and the second is the delta spline technique (Boneva, Kendall & Stepanov 1971). Both methods may be thought of as an approximation to an integral determined according to the Monte Carlo procedure. Since the Monte Carlo method is known to give reasonable estimates of multiple integrals with fewer points than finite difference methods often require, it is plausible to expect a reduction in work if the statistical smoothing methods are used. We call this method smoothed particle hydrodynamics (SPH).

In this paper we first give a detailed description of the smoothing method and establish conditions which guide the choice of the smoothing kernel. Static spherical polytropes are then studied by relaxing from an initial non-spherical configuration with a damping term in the equations of motion. The free non-spherical oscillations of polytropes are then examined. Finally the departures from spherical symmetry produced by uniform rotation and magnetic fields in polytropes are determined and compared with results from perturbation theory.

## 2 Recovering distributions and body forces

### 2.1 THE DENSITY DISTRIBUTION

The equation of motion of the  $j$ th element of fluid with volume  $\Delta v_j$ , centre of mass  $\mathbf{r}_j$  and density  $\rho_j$  is

$$\rho_j \Delta v_j \frac{d^2 \mathbf{r}_j}{dt^2} = -\Delta v_j \nabla P + \rho_j \Delta v_j \mathbf{F}_j, \quad (2.1)$$

or

$$\frac{d^2 \mathbf{r}_j}{dt^2} = -\frac{1}{\rho_j} \nabla P + \mathbf{F}_j, \quad (2.2)$$

where  $\mathbf{F}_j$  is the body force acting on the element of fluid and  $\nabla P$  is the pressure gradient at  $\mathbf{r}_j$ . Since in our approximation the element of fluid is described dynamically by a point, we shall call it a particle, and (2.2) the equation of motion of the  $j$ th particle.

It is convenient to begin our analysis by considering the calculation of a smoothed

\* Leon Lucy has proposed and experimented with a similar method. See the acknowledgment.

density from a set of points, the various  $\mathbf{r}_j$  distributed according to the density. Following Parzen (1962), we consider a smoothed density  $\rho_s(\mathbf{r})$  defined by

$$\rho_s(\mathbf{r}) = \int W(\mathbf{r} - \mathbf{r}') \rho(\mathbf{r}') d\mathbf{r}', \quad (2.3)$$

where  $W$  is a function satisfying the condition

$$\int W(\mathbf{r}) d\mathbf{r} = 1, \quad (2.4)$$

where the integration is over all space.

If  $\rho(\mathbf{r}')$  is unknown, (2.3) cannot be evaluated, but if we have a set of  $N$  points ( $\mathbf{r}_1, \mathbf{r}_2, \dots, \mathbf{r}_N$ ) distributed according to  $\rho$ , the integral can be evaluated by the Monte Carlo method (Hammersley & Handscomb 1964). Thus, defining  $\rho_N(\mathbf{r})$  by

$$\rho_N(\mathbf{r}) = \frac{M}{N} \sum_{j=1}^N W(\mathbf{r} - \mathbf{r}_j), \quad (2.5)$$

where

$$M = \int \rho(\mathbf{r}) d\mathbf{r}, \quad (2.6)$$

we find, with  $E$  denoting the expectation

$$E[\rho_N(\mathbf{r})] \equiv \frac{1}{M^N} \int \dots \int \rho_N(\mathbf{r}) \prod_{i=1}^N \rho(\mathbf{r}_i) d\mathbf{r}_i = \rho_s(\mathbf{r}). \quad (2.7)$$

In our numerical procedure only one sample distribution is produced each time. The equality (2.7) is therefore to be understood as implying that if we were to create an ensemble of models, each starting with a different array of points consistent with the initial conditions, then the ensemble average of  $\rho_N(\mathbf{r})$  would be  $\rho_s(\mathbf{r})$ .

The error involved in replacing  $\rho_s(\mathbf{r})$  by  $\rho_N(\mathbf{r})$  is  $\pm\sigma$ , where  $\sigma$  is defined by

$$\begin{aligned} \sigma^2 &= E[(\rho_N(\mathbf{r}) - \rho_s(\mathbf{r}))^2] \\ &= \frac{M^2}{N^2} \sum_j W^2(\mathbf{r} - \mathbf{r}_j) - \frac{1}{N} \left[ \frac{M}{N} \sum_j W(\mathbf{r} - \mathbf{r}_j) \right]^2 \end{aligned} \quad (2.8)$$

To complete the chain of analysis it is necessary to show that a  $W(\mathbf{r})$  can always be chosen so that, as  $N$  increases,  $\rho_s(\mathbf{r})$  becomes a better approximation to  $\rho(\mathbf{r})$ . We establish this result in the next section.

## 2.2 CHOOSING THE KERNEL $W(\mathbf{r})$

Intuitively it seems reasonable to expect that  $W(\mathbf{r})$  can be made more like  $\delta(\mathbf{r})$  as  $N$  becomes larger. If this is the case then

$$\rho_s(\mathbf{r}) \rightarrow \rho(\mathbf{r}) \text{ as } N \rightarrow \infty.$$

To make this result more precise it is convenient to write  $W(\mathbf{r})$  in the form

$$W(\mathbf{r}) = \frac{1}{h^3} K(\mathbf{r}/h), \quad (2.9)$$

where  $h$  is a parameter with the dimensions of length and the space is assumed to be three dimensional. By an easy generalization of a theorem due to Parzen (1962) we find that if

$$h \rightarrow 0 \text{ as } N \rightarrow \infty$$

and if  $K(\mathbf{u})$  is a Borel function satisfying

$$\int K(\mathbf{u}) d\mathbf{u} = 1, \quad |\mathbf{u}^2 K(\mathbf{u})| \rightarrow 0 \text{ as } |\mathbf{u}| \rightarrow \infty, \quad \int |K(\mathbf{u})| d\mathbf{u} < \infty$$

where the integrals are over all space, then

$$\rho_N(\mathbf{r}) \rightarrow \rho(\mathbf{r}) \text{ as } N \rightarrow \infty.$$

It proves convenient to choose  $W(\mathbf{r})$  to be an even function. Typical examples of kernel functions in three dimensions are

$$(i) \left( \frac{1}{\pi h^2} \right)^{3/2} \exp(-r^2/h^2) \quad (ii) \frac{3H(1-|\mathbf{r}|/h)}{4\pi h^3} \quad (iii) \frac{S(|\mathbf{r}|/h)}{h^3} \quad (2.10)$$

where  $H$  is the Heaviside step function and  $S$  is the spherical delta spline discussed in Appendix 1. Each of the functions in (2.10) is a member of a sequence of functions which represents the delta function.

In addition to requiring  $\rho_N(\mathbf{r}) \rightarrow \rho(\mathbf{r})$  we require that  $\sigma$  should be as small as possible. To satisfy these conditions we choose  $h$  by minimizing the functional

$$L(\mathbf{r}) = \{E[\rho_N(\mathbf{r})] - \rho(\mathbf{r})\}^2 + E[(\rho_N(\mathbf{r}) - \rho_s(\mathbf{r}))^2] \\ = E[(\rho_N(\mathbf{r}) - \rho(\mathbf{r}))^2]. \quad (2.11)$$

Using (2.5) we find

$$L(\mathbf{r}) = \frac{M}{N} \int W^2(\mathbf{r}-\mathbf{r}') \rho(\mathbf{r}') d\mathbf{r}' + \left(1 - \frac{1}{N}\right) \left[ \int W(\mathbf{r}-\mathbf{r}') \rho(\mathbf{r}') d\mathbf{r}' \right]^2 \\ + \rho^2(\mathbf{r}) - 2\rho(\mathbf{r}) \int W(\mathbf{r}-\mathbf{r}') \rho(\mathbf{r}') d\mathbf{r}'. \quad (2.12)$$

Since  $W(\mathbf{r}-\mathbf{r}')$  is strongly peaked at  $\mathbf{r} = \mathbf{r}'$ , we can expand  $\rho(\mathbf{r}')$  about  $\mathbf{r}$ . Keeping only the dominant terms, we find

$$L(\mathbf{r}) \sim \frac{M}{N} \rho(\mathbf{r}) \int W^2(\mathbf{r}') d\mathbf{r}' + \left\{ \frac{\nabla^2 \rho}{6} \int W(\mathbf{r}') \mathbf{r}'^2 d\mathbf{r}' \right\}^2. \quad (2.13)$$

Using (2.9) the minimum of  $L(\mathbf{r})$  is found to occur at

$$h^7 = \frac{27}{N} \frac{M\rho}{(\nabla^2 \rho)^2} \frac{\int K^2(\mathbf{u}) d\mathbf{u}}{\left\{ \int K(\mathbf{u}) u^2 d\mathbf{u} \right\}^2}. \quad (2.14)$$

Since  $\rho$  is unknown (2.14) cannot be used directly except to infer

$$h \propto 1/N^{1/7} \text{ and } L_{\min} \propto 1/N^{4/7}.$$

We find an appropriate choice of  $h$  to be given by

$$h = b (\langle \mathbf{r}^2 \rangle - \langle \mathbf{r} \rangle^2)^{1/2}, \quad (2.15)$$

where  $b$  is adjustable and

$$\langle c(\mathbf{r}) \rangle = \frac{\int \rho c d\mathbf{r}}{M} \doteq \frac{1}{N} \sum_j c(\mathbf{r}_j).$$

In the problems we consider, the derivative of the smoothed function is required to be continuous. For this reason the second of the kernel functions in (2.10) is not useful. Of the other possible kernel functions we have concentrated on the Gaussian and spline functions.

To decide between the Gaussian and the spline kernels we took a known distribution and distributed a set of points. The goodness of fit  $[\rho_N(\mathbf{r}) - \rho(\mathbf{r})]^2$  was then evaluated for various values of  $b$ . For forty points there is negligible difference between the two kernels, but for 80 points the Gaussian was much more accurate. For this reason we prefer the Gaussian kernel and use it for the results reported here.

For our stellar models we choose  $b$  by requiring the smoothed particle model to fit the known density of the spherically symmetric hydrostatic model. More elaborate procedures could be used but we have found those described to be successful for the models considered.

### 2.3 THE GRAVITATIONAL POTENTIAL

We use the gravitational potential  $\phi$  defined by

$$\phi = -G \int \frac{\rho_N(\mathbf{r}') d\mathbf{r}'}{|\mathbf{r} - \mathbf{r}'|}. \quad (2.16)$$

Using (2.5)

$$\phi = -\frac{GM}{N} \sum_{j=1}^N \int \frac{W(\mathbf{r}' - \mathbf{r}_j) d\mathbf{r}'}{|\mathbf{r} - \mathbf{r}'|}. \quad (2.17)$$

$$I_j = \int \frac{W(\mathbf{r}' - \mathbf{r}_j) d\mathbf{r}'}{|\mathbf{r} - \mathbf{r}'|}, \quad (2.18)$$

can be evaluated easily noting that

$$\nabla^2 I_j = -4\pi W(\mathbf{r} - \mathbf{r}_j). \quad (2.19)$$

We find

$$\nabla \phi = -\frac{GM}{N} \sum_{j=1}^N \left\{ -\frac{4\pi}{u_j^2} \int_0^{u_j} W(u) u^2 du \right\} \nabla u_j, \quad (2.20)$$

where

$$u_j = \mathbf{r} - \mathbf{r}_j.$$

For the Gaussian  $W$  defined by (2.10) (i) with  $f = 1/h^2$

$$\nabla\phi = -\frac{GM}{N} \sum_{j=1}^N \frac{2}{u_j} \left(\frac{f}{\pi}\right)^{1/2} \left[ \exp(-fu_j^2) - \frac{1}{u_j} \int_0^{u_j} \exp(-fu^2) du \right] \nabla u_j \quad (2.21)$$

and

$$I_j = \frac{2}{u_j} \left(\frac{f}{\pi}\right)^{1/2} \int_0^{u_j} \exp(-fu^2) du.$$

The equivalent formulae for the delta spline  $W$  involve polynomials, and are easier to evaluate.

## 2.4 GENERAL DISTRIBUTIONS

To find the smoothed version of any other scalar (or vector) field  $A(\mathbf{r})$ , we define the smoothed field  $A_s(\mathbf{r})$  by

$$A_s(\mathbf{r}) = \int W(\mathbf{r} - \mathbf{r}') A(\mathbf{r}') d\mathbf{r}', \quad (2.22)$$

where, in general, the kernel differs from that in (2.3). Then an estimate of  $A_s(\mathbf{r})$  is

$$A_N(\mathbf{r}) = \frac{M}{N} \sum_{j=1}^N W(\mathbf{r} - \mathbf{r}_j) \frac{A(\mathbf{r}_j)}{\rho(\mathbf{r}_j)}. \quad (2.23)$$

The error in this estimate is  $\pm\sigma$  where now

$$\sigma^2 = \frac{M^2}{N^2} \sum_j W^2(\mathbf{r} - \mathbf{r}_j) \frac{A^2(\mathbf{r}_j)}{\rho^2(\mathbf{r}_j)} - \frac{1}{N} A_N^2. \quad (2.24)$$

The approximations involved become better when  $A(\mathbf{r})$  is distributed similarly to the density. This is the case for temperature and entropy, but for the magnetic field it is not in general true. To deal with this case importance sampling is useful and we discuss its application in the next subsection. Where the field has known symmetry properties antithetic variables can be used to improve the accuracy.

## 2.5 THE MAGNETIC FIELD AND CURRENT

According to the prescription given in Section 2.4 an estimate of the magnetic field is given by

$$\mathbf{B}_N(\mathbf{r}) = \frac{M}{N} \sum_{j=1}^N W(\mathbf{r} - \mathbf{r}_j) \frac{\mathbf{B}_j}{\rho_j}, \quad (2.25)$$

and an estimate of the current by

$$\mathbf{J}_N(\mathbf{r}) = \epsilon_0 c^2 \frac{M}{N} \sum_j \nabla W \times \frac{\mathbf{B}_j}{\rho_j}. \quad (2.26)$$

However it is usually the case that there is field inside and outside the star and (2.25) is then a poor approximation to  $\mathbf{B}_s(\mathbf{r})$ , and (2.26) is an even poorer approximation to  $\mathbf{J}_s(\mathbf{r})$ . To

improve the approximation we use importance sampling (Hammersley & Handscomb 1964) in the form

$$\mathbf{B}_s(\mathbf{r}) = \mathbf{B}_0(\mathbf{r}) + \int W(\mathbf{r} - \mathbf{r}') [\mathbf{B}(\mathbf{r}') - \mathbf{B}_0(\mathbf{r}')] d\mathbf{r}', \quad (2.27)$$

where  $\mathbf{B}_0(\mathbf{r})$  is an approximation to  $\mathbf{B}(\mathbf{r})$ . To obtain this approximation we solve

$$\epsilon_0 c^2 \nabla \times \mathbf{B}_0 = \mathbf{J}_N(\mathbf{r}), \quad (2.28)$$

in the form

$$\mathbf{B}_0 = \mathbf{B}_{\text{ext}} + \frac{1}{4\pi\epsilon_0 c^2} \int \frac{\mathbf{J}_N(\mathbf{r}') \times (\mathbf{r} - \mathbf{r}')}{|\mathbf{r} - \mathbf{r}'|^3} d\mathbf{r}', \quad (2.29)$$

where  $\mathbf{B}_{\text{ext}}$  is any superimposed external field. It could, for example, be the field permeating an interstellar cloud from which a star is forming. Substituting (2.26) into (2.29) we find

$$\mathbf{B}_0(\mathbf{r}) = \mathbf{B}_{\text{ext}} - \frac{M}{4\pi N} \sum_{j=1}^N \left[ \left( \frac{\mathbf{B}_j}{\rho_j} \cdot \frac{\partial}{\partial \mathbf{r}} \right) \frac{\partial I_j}{\partial \mathbf{r}_j} - \frac{4\pi}{\rho_j} \mathbf{B}_j W(\mathbf{r} - \mathbf{r}_j) \right], \quad (2.30)$$

where  $I_j$  is defined by (2.18).

For the Gaussian kernel (2.10) (i) with  $f = 1/h^2$ , the approximate field becomes

$$\mathbf{B}_0(\mathbf{r}) = \mathbf{B}_{\text{ext}} + \frac{M}{N} \sum_j \left( \frac{f}{\pi} \right)^{3/2} \left\{ \begin{aligned} & \frac{\mathbf{B}_j}{\rho_j} \left[ \exp(-fu^2) - \frac{1}{u^3} \int_0^u \exp(-fv^2) v^2 dv \right] \\ & + \mathbf{u} \left( \frac{\mathbf{B}_j \cdot \mathbf{u}}{\rho_j u} \right) \left[ \frac{3}{u^4} \int_0^u \exp(-fv^2) v^2 dv - \frac{\exp(-fu^2)}{u} \right] \end{aligned} \right\} \quad (2.31)$$

where  $\mathbf{u} = \mathbf{u}_j = \mathbf{r} - \mathbf{r}_j$ .

The field we use is

$$\mathbf{B}_N(\mathbf{r}) = \mathbf{B}_0(\mathbf{r}) + \frac{M}{N} \sum_j \frac{W(\mathbf{r} - \mathbf{r}_j)}{\rho_j} \{\mathbf{B}(\mathbf{r}_j) - \mathbf{B}_0(\mathbf{r}_j)\} \quad (2.32)$$

and the current is obtained from the curl of (2.32). Thus

$$\mathbf{J}_N(\mathbf{r}) = \frac{\epsilon_0 c^2 M}{N} \sum_j \frac{\nabla W}{\rho_j} \times \{2\mathbf{B}(\mathbf{r}_j) - \mathbf{B}_0(\mathbf{r}_j)\} + \mathbf{J}_{\text{ext}}(\mathbf{r}), \quad (2.33)$$

where  $\mathbf{J}_{\text{ext}}$  is the current associated with  $\mathbf{B}_{\text{ext}}$ . This procedure, as we show later, gives a good fit to the current and the field.

### 3 Equations of motion

The equations of motion of the fluid particles for a uniformly rotating polytrope of index  $n$ , with an internal magnetic field  $\mathbf{B}$  are

$$\frac{d^2 \mathbf{r}_j}{dt^2} = -\Gamma \frac{d\mathbf{r}_j}{dt} - K \rho_j^{1/n-1} \frac{(1+n)}{n} \nabla \rho - \nabla \phi - \boldsymbol{\Omega} \times (\boldsymbol{\Omega} \times \mathbf{r}) - 2\boldsymbol{\Omega} \times \frac{d\mathbf{r}_j}{dt} + \frac{\mathbf{J} \times \mathbf{B}}{\rho}, \quad j = 1, 2, \dots, N \quad (3.1)$$



where the pressure  $P = K\rho^{1+1/n}$ ,  $\Omega$  is the angular velocity,  $\mathbf{B}$  the magnetic field and  $\mathbf{J}$  the current. The damping term  $\Gamma d\mathbf{r}_j/dt$  has been introduced to allow static models to be calculated. For the rotating models considered here only the static structure is required, and the Coriolis term can be dropped. Using the dimensionless variables  $\mathbf{x}_j$ ,  $D$ ,  $\tau$ ,  $\mathbf{b}$  defined by

$$\rho = \lambda D, \quad \mathbf{r}_j = \alpha \mathbf{x}_j, \quad t = \beta \tau, \quad \mathbf{B} = B \mathbf{b} \quad (3.2)$$

where

$$\alpha^2 = \frac{(n+1)K\lambda^{1/n-1}}{4\pi G}, \quad \beta^2 = \frac{\alpha^2 n}{K\lambda^{1/n}(1+n)}, \quad (3.3)$$

and  $\lambda$  and  $B$  can be chosen for convenience. (3.1) becomes, on dropping the Coriolis term,

$$\frac{d^2 \mathbf{x}_j}{d\tau^2} = -\frac{\gamma d\mathbf{x}_j}{d\tau} - D_j^{1/n-1} \nabla D_j - \frac{n}{4\pi} \nabla \Phi - \omega^2 \mathbf{i} \times (\mathbf{i} \times \mathbf{x}_j) + \eta \frac{(\nabla \times \mathbf{b}) \times \mathbf{b}}{D_j}, \quad (3.4)$$

where  $\gamma$  is a new damping constant

$$\Omega = \left( \frac{4\pi G \lambda}{n} \right)^{1/2} \omega \mathbf{i}, \quad \eta = \frac{\epsilon_0 c^2 n B^2}{4\pi G \lambda^2 \alpha^2}, \quad (3.5)$$

and  $\Phi$  is the scaled gravitational potential where

$$\Phi = \frac{\phi}{G\lambda\alpha^3} = \frac{\phi Q}{GM}$$

and we have chosen the value of  $Q = \int D(\mathbf{x}) d\mathbf{x}$  such that were the representations of integrals by sums in Section 2 to be exact, then  $D(0)$  would equal unity and  $\lambda$  would be the central density. Our scaled variables are therefore similar to the usual polytropic variables (Chandrasekhar 1939). However, since in our models  $D(0) \neq 1$ , our length scale is related to the polytropic variable  $\xi$  by  $\xi = D(0)^{(n-1)/2n} |\mathbf{x}|$ .

For the models considered here the magnetic field variation is calculated in the flux freezing approximation

$$\frac{d}{dt} \left( \frac{\mathbf{B}}{\rho} \right) = \left( \frac{\mathbf{B}}{\rho} \cdot \nabla \right) \mathbf{v}, \quad (3.6)$$

where  $d/dt$  is a derivative following the motion. To integrate this equation forward we replace  $\mathbf{v}$  by the smoothed velocity field. Equation (3.6) has the advantage that it automatically generates the quantity  $\mathbf{B}/\rho$  required at each fluid element to produce the smoothed field.

## 4 Numerical tests – spherical models

### 4.1 CONSTRUCTION OF STATIC MODELS

To construct a static model we follow the damped motion of a set of particles from some initial distribution of position and velocity until the system comes to rest. Typically the particles were initially at rest, distributed in space either according to a random Gaussian distribution or alternatively on a spherically symmetric cubic lattice. In the former case the



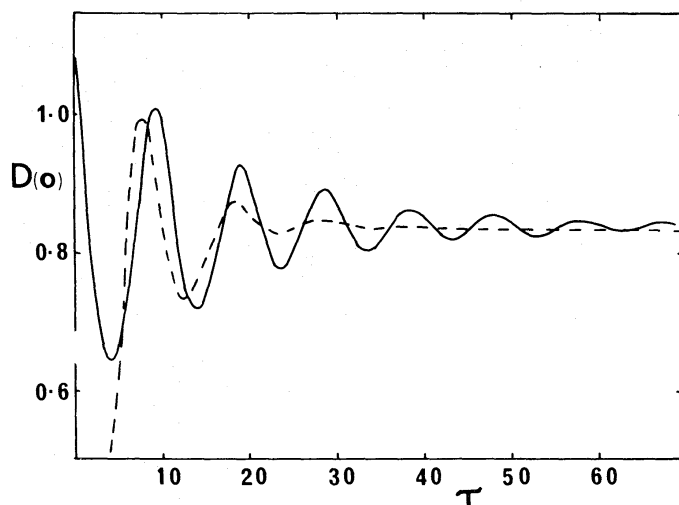


**Figure 1.** The central density  $D(0)$  as a function of time  $\tau$  for two damped hydrodynamic sequences. The initial configurations are given in the text.

initial coordinates of the particles were adjusted so that the centre of mass was at the centre of the coordinate system. As a check, the position and velocity of the centre of mass were monitored throughout the calculations.

The approach to equilibrium for two initial configurations with different degrees of damping is illustrated in Fig. 1 for a polytrope of index 1. The solid line represents the behaviour of  $D(0)$  as a function of the scaled time  $\tau$ , in a sequence that commences with 33 particles on a cubic lattice and  $\gamma = 0.05$ . The broken curve shows a sequence, with  $\gamma = 0.15$ , commencing with 40 particles distributed normally about the origin.

The models finally obtained are found to be nearly independent of both the damping, the initial configuration, and the number of particles. These model sequences commence, of course, with a good deal of spherical symmetry. Quite irregular initial distributions can also be successfully treated. Fig. 2(a) shows the density profile in the  $(X, Y)$  plane of an initially non-spherically symmetric distribution which leads to the symmetric distribution of Fig. 2(b) representing a polytrope of index 1.

## 4.2 STATIC STRUCTURE

Polytropes of index 1 and 1.5, constructed using about 40 particles and a wide range of smoothing constant  $b$  (defined by equation 2.15) were found to have density profiles which matched the true density to within a few per cent over the bulk of the star. The density profile in the outermost 10 per cent of the polytropic radius for the polytrope of index 1, however, reflects the nature of the smoothing function rather more than it does the actual distribution of matter. The size of this region can be decreased by employing a larger number of particles.

Sequences that commenced with a high degree of spherical symmetry yielded similarly highly symmetric polytropes. The departure from spherical symmetry in other cases was less than 2 per cent.

Polytropes of index 2.5 were also constructed employing both a range in the number of particles and in the value of the smoothing constant  $b$ . In Fig. 3 we display the appropriately scaled density profiles of two such models. The curve represents the true density for  $n = 2.5$  while the filled circles show the density profile of a model constructed with  $N = 80$ . Since this model is highly symmetrical the density profile along only one axis is shown. Also

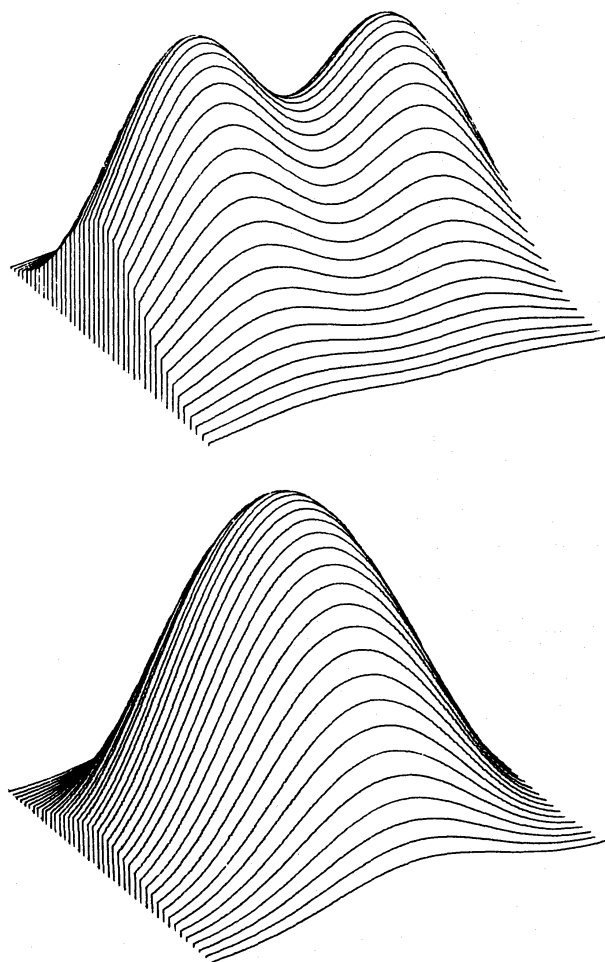


**Figure 2.** An example of initial and final smoothed density in the  $x,y$  plane for a polytrope of index 1. The initial state was a superposition of two Gaussian density distributions.

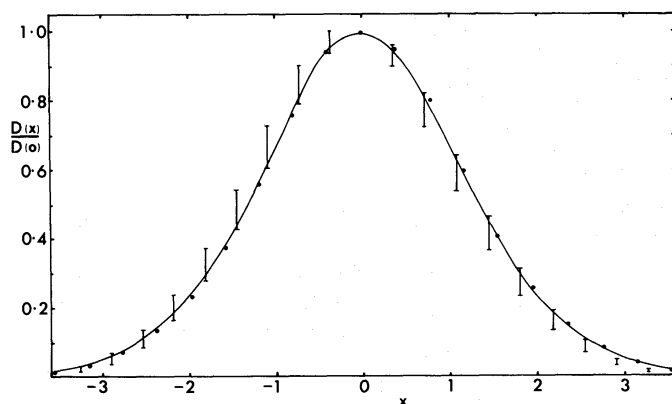


**Figure 3.** Density profiles for a polytrope of index 2.5. The Emden density is shown: —; the 80-particle SPH is shown: ..... The variation in density for a given  $x$  along the  $x,y,z$  axes is indicated by the size of the filled circle. The analogous variation for 40 particles is shown by the bar.

indicated in Fig. 3 is the less symmetrical density profile of a model constructed with one half as many particles. The range in density at points on each of the three coordinate axes for this model is indicated by the vertical bars. The density profiles in this case fit the true density more closely than might appear from the figure. Along each of the coordinate axes

**Table 1.** Parameters of polytropes of index 2.5.

$N$	40	40	40	40	40	80	200	200	200
$1/b^2$	0.5	1.0	1.5	2.0	2.5	2.0	1.6	2.0	3.0
$1/h^2$	0.35	0.60	1.05	1.69	2.81	1.01	0.67	0.79	1.19
$D(0)$	0.72	1.22	1.97	2.97	4.92	1.52	1.06	1.08	1.34
$\langle \xi^2 \rangle$	1.17	1.88	2.15	2.27	2.31	2.55	2.47	2.65	3.01

the density profile is quite good, but the peak value is offset from the origin. Nevertheless, the improvement achieved by increasing the number of particles from 40 to 80 is remarkable and surpasses the  $\sqrt{N}$  improvement we would expect in Monte Carlo integrations. This is probably due to 40 particles being intrinsically too few.

Some brief details of various models for  $n=2.5$  are given in Table 1. In each case the sequence commenced with a Gaussian distribution of particles about the origin. Although the final values of  $D(0)$  vary with both the smoothing parameter and the number of particles, in each case the density profile after dividing by  $D(0)$  is similar. Also displayed in Table 1 are the mean squared radial position of the particles given by

$$\langle \xi^2 \rangle = \frac{1}{N} \sum \xi_j^2 \cong \int \rho \xi^2 dv / \int \rho dv.$$

These values are smaller than the value of 4.8 obtained by performing the integrations using the density profile in the above expression. This discrepancy is not surprising since the integrand  $\rho \xi^4$  has a sharp maximum beyond the position of the bulk of our particles.

### 4.3 UNDAMPED OSCILLATIONS

Several hydrodynamic sequences were followed with damping excluded. These were found to oscillate in a mixture of modes reflecting the initial state of the model. In each case a dominant period of oscillation of the central density was manifest. This matched the periods of oscillation of polytropes of index  $n$  in the range 1–2.5 given by Kopal (1938) to within 10 per cent for  $N \sim 40$ . This error can be reduced by using more particles. During extended runs over many cycles of large amplitude oscillations ( $\delta D(0)/D(0) \sim 0.3$ ) the total energy  $E$  of systems with  $N \sim 40$  was found to oscillate with  $|\delta E/E| \lesssim 0.1$ . This error is consistent with replacing integrals by sums according to the Monte Carlo procedure.

## 5 Numerical tests – non-spherical models

### 5.1 UNIFORMLY ROTATING POLYTROPES

Uniformly rotating polytropes were studied to determine the accuracy with which the technique reproduced a non-spherical structure.

In Fig. 4 the polar and equatorial density profiles are shown for a rapidly rotating polytrope of index 1.5 for which  $\omega^2 = 0.024$ . The figure also shows the density profiles for the same model obtained using the approximation technique of Monaghan & Roxburgh (1965). It is clear that the agreement is good. All models were found to be symmetric about the rotation axis and the equator to within 5 per cent.

Because our models do not have  $D(0) = 1$ , the parameter  $\alpha$  of Monaghan & Roxburgh is related to our  $\omega^2$  by  $\alpha = 2\omega^2/nD(0)$ . The model shown is therefore on the verge of breakup. Since our method does not produce fluid particles near the edge, the critical  $\omega$  corre-

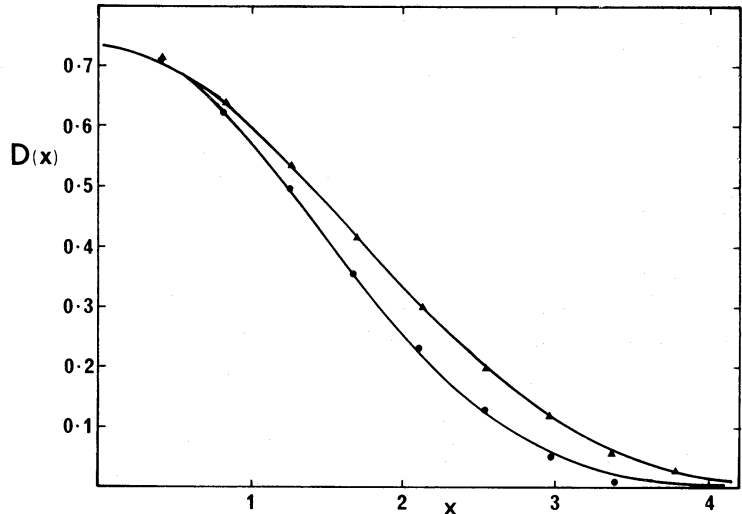


**Figure 4.** The density profiles for a uniformly rotating polytrope of index 1.5. The SPH results are shown thus: polar density: lower curve; equatorial density: upper curve. Perturbation analysis (Monaghan & Roxburgh 1965) shown by ••••• and ▲▲▲▲.

sponding to breakup cannot be determined accurately. Of course, with more particles, and therefore a smaller  $h$ , the critical  $\omega$  can be calculated as accurately as desired. Alternatively test particles could be introduced.

5.2 MAGNETIC POLYTROPES

The static structure of polytropes with both poloidal and toroidal fields was studied by starting with a static, non-rotating, polytrope and then superimposing the field. The polytrope was then allowed to relax to a static structure. Because the main purpose of this study was to explore the numerical method we chose initial fields which were known solutions of

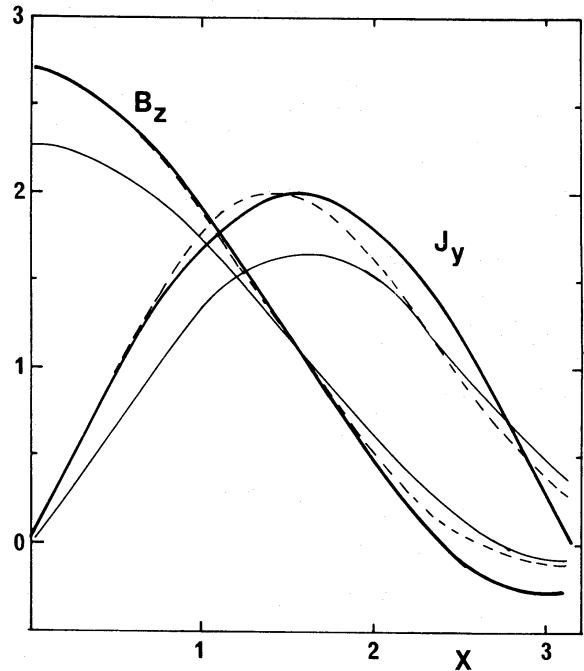


**Figure 5.** Poloidal magnetic field and current in a polytrope of index 1. Perturbation analysis (Monaghan 1965) shown thus: ———. The smoothed initial field and current shown thus: ----- . The final static field and current shown thus: - · - · - .

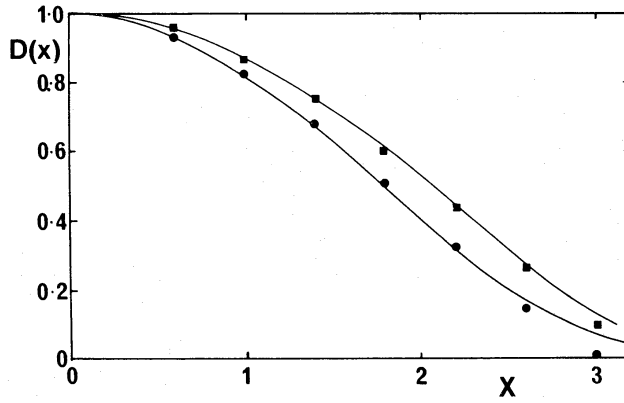


**Figure 6.** Density profiles for a polytrope of index 1 with a dipole poloidal field. Perturbation analysis (Monaghan 1965) shown thus: polar density: ●●●●; equatorial density: ■■■. The SPH density shown thus: ———. The full field smoothing method has been used.

the first-order perturbation equations. The poloidal field was taken from Monaghan (1965) and the toroidal field from Roxburgh (1966).

In Fig. 5 we show the initial field and current on the  $x$  axis calculated from the analytical expression for a dipole field in a polytrope of index 1. Also shown is the initial and final smoothed field and current calculated according to the procedure of Section 2.5. The agreement between the initial field and its smoothed equivalent is very good. We believe it could be further improved by adjusting the smoothing parameter  $b$ , or by adopting a different value of this parameter for each component of the magnetic field.

The analytical equilibrium field is based on a first-order perturbation analysis which assumes the field can be constructed from a non-perturbed density. Since we find density perturbations of  $\sim 10$  per cent, we expect the final field to differ from the first-order perturbation results by quantities of this order. The difference between the initial and final field and current shown in Fig. 5 is therefore not unexpected.

In Fig. 6 the equatorial and polar density profiles are shown for both the present numerical calculations, and for the first-order perturbation results. Since our models have  $D(0) \neq 1$ , and a field and current which differ from the analytical one by approximately a scale factor, the relation between  $\eta$  and the factors  $\varpi$  and  $k$  of Monaghan (1965) is approximately

$$\varpi = \frac{\eta}{nk^2 D(0)^{1+1/n}} \left( \frac{\text{computed } B_z(0)}{\text{analytical } B_z(0)} \right)^2.$$

The agreement between the first-order perturbation results and our numerical results is very good. Small changes, of the order of 10 per cent of the deviations from the unperturbed density, are to be expected because of errors in the perturbation method, but this has a negligible effect on the density profiles.

The toroidal field investigated is zero outside the polytrope and the smoothed field can be obtained satisfactorily without using the importance sampling device of Section 2.5. With 40 particles in a polytrope of index 1 the initial smoothed field reproduced the analytical field to within  $\leq 5$  per cent.

During the calculations the constancy of the magnetic flux was monitored and found to remain constant to within 2 per cent.

## 6 Computational requirements

All of the sequences described in this paper were stored in 60–90K bytes of core storage in an IBM 360/165. A typical  $N=40$  sequence with no magnetic field requires about 0.25 s per

time step and about 200 time steps (50 s) per model. The time step is fixed by calculating the minimum of  $h/v_{\max}$ ,  $(h/F_{\max})^{1/2}$  and  $h/D^{1/2n}$  where  $v_{\max}$  is the maximum particle velocity,  $F_{\max}$  the maximum force and the last criterion is based on the speed of sound. The minimum is then multiplied by a constant. If this constant is in the range 0.1–0.5 the integration is stable without requiring excessive time. The time can be halved by storing the current forces and densities at the particle positions. We are currently performing calculations for dynamical sequences leading to fission. These require approximately four minutes of computing time for an 80-particle configuration.

## Conclusions

The results of this study show that the smoothed particle method is a simple technique which gives satisfactory results for oscillating polytropes, and for polytropes which relax from a non-spherical initial state to a spherical final state. Rotation and magnetic fields may be included without difficulty, and the comparison with the perturbation results shows that moderate distortion can be reproduced accurately. Structure on a finer scale or greater accuracy can always be obtained by increasing the number of particles and by using the devices known to improve Monte Carlo integration methods.

## Acknowledgment

In a lecture give at the Institute of Astronomy, Cambridge in 1976 Leon Lucy discussed the use of smoothing techniques for hydrodynamic codes. His ideas were adumbrated to us by our colleagues, but the mathematical development in this paper is independent of his work.

## References

- Bartlett, M. S., 1963. *Sankhya (A)*, **25**, 245.  
 Boneva, L. I., Kendall, D. & Stepanov, I., 1971. *J. R. stat. Soc.*, **33**, 1.  
 Chandrasekhar, S., 1939. *An introduction to the study of stellar structure*, p. 87. University of Chicago Press.  
 Hammersley, J. M. & Handscomb, D. C., 1964. *Monte Carlo methods*, Methuen, London.  
 Kopal, Z., 1938. *Mon. Not. R. astr. Soc.*, **99**, 33.  
 Monaghan, J. J., 1965. *Mon. Not. R. astr. Soc.*, **131**, 105.  
 Monaghan, J. J. & Roxburgh, I. W., 1965. *Mon. Not. R. astr. Soc.*, **131**, 13.  
 Parzen, E., 1962. *Ann. Math. Stat.*, **33**, 1065.  
 Pasta, J. R. & Ulam, S., 1959. *Mathematical tables and other aids to computation*, **13**, 1.  
 Roxburgh, I. W., 1966. *Mon. Not. R. astr. Soc.*, **132**, 347.

## Appendix

In one dimension the simplest representation of a sample is by a histogram. To smooth the histogram the constraints of minimizing the slope, while retaining reproducibility of the data, can be used. The resulting smoothing function is the delta spline of Boneva, Kendall & Stepanov (1971).

In three dimensions there are various possible generalizations. Our experiments have been based on the following.

Around a sample point construct the unit ball, i.e. the sphere of unit radius. This is one generalization of the unit histogram. Surround the ball by concentric shells of radius  $r_i = i$ . Now construct the spherical delta spline  $S(r)$  by the rules

$$\text{Min } 4\pi \int_{r_i}^{r_{i+1}} \left( \frac{\partial S}{\partial r} \right)^2 r^2 dr \text{ with } 4\pi \int_{r_i}^{r_{i+1}} S r^2 dr = \delta_{i0} \quad i = 1, 2, 3.$$

These rules ensure minimization of the slope with the constraint that the integral over all space is equal to the contribution from within the unit ball. The resulting set of equations is easily solved and the spherical delta spline is found to oscillate with an exponentially decreasing amplitude.

An alternative we haven't experimented with is based on the subdivision of the space into cubes. Then the function to be minimized is  $(\partial^3 S / \partial x \partial y \partial z)^2$  and the delta spline becomes just a product of one-dimensional delta splines.